Chapter 3

Elaboration to APTO and AETD

3 Elaboration to APTO and AETD

3.1 The AD

3.1.1 Ligand Effects

The Sharpless Asymmetric Dihydroxylation[32] (AD) converts an alkene to a vicinal diol. The reaction was the forerunner to the AA and involves similar conditions without a nitrogen source which eliminates the issue of regio-selectivity. The mechanism[32] of the reaction occurs by *syn*-addition, where both alcohols are delivered to the same face of the compound, therefore when an (*E*)-alkene is reacted a *syn*-diol is formed. There are two possible products that may form in the reaction: the desired diol **22**, where the alcohols are delivered to the front face of alkene ***E*-23**, and the diastereoisomeric diol ***dia*-22**, where the alcohols are delivered to the back face of alkene ***E*-23** (Figure 3.1). These products are referred to as 3,4-*anti*-diol **22** and 3,4-*syn*-diol ***dia*-22** where the terms *anti*- and *syn*- refer to the relative stereochemistry of the C_3 and C_4 substituents.

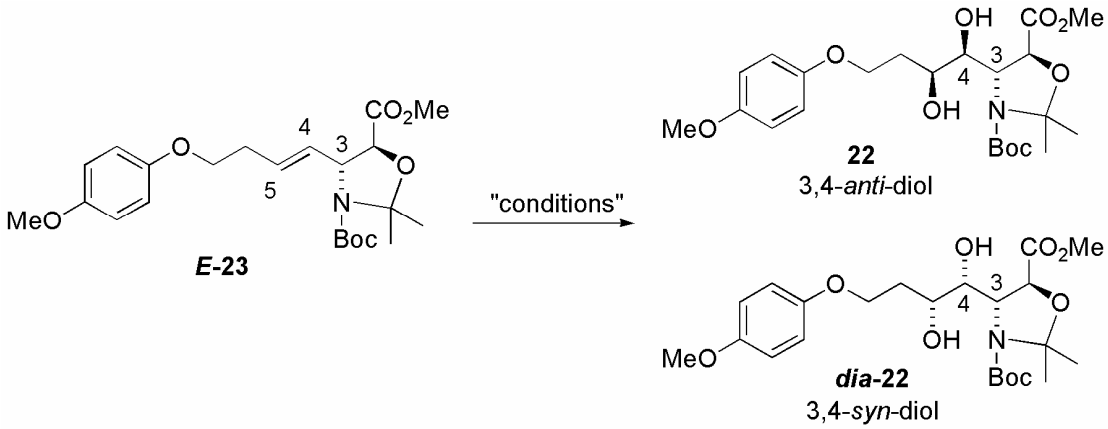

Figure 3.1 Dihydroxylation.

As in the AA, correct choice of reagents linked with smart substrate design can induce high selectivity in the product. The substrate was designed to incorporate

the *p*-methoxyphenyl ether protecting group due to its ability to boost enantio-selectivity in the AD[28] and its ease of removal using ammonium cerium(IV) nitrate.[57]

Many researchers have observed that chiral substrates have "intrinsic diastereofacial selectivity" where pre-existing chirality in the substrate favours diol addition to one face over the other.[32] One such study by Morikawa and Sharpless[58] involved the AD of chiral alkene **91** (Figure 3.2). The dihydroxylation in the absence of a chiral ligand formed 3,4-*anti*-diol **92** and 3,4-*syn*-diol ***dia*-92** in a 2.6 : 1 ratio (Figure 3.3, entry 1). It was proposed that addition to the back face of alkene **91** is favoured since the approach is less sterically congested. The authors went on to study the effect of including chiral ligands in the reaction. The AD mnemonic was used to predict that formation of 3,4-*anti*-diol **92** would be favoured by DHQD ligands and formation of 3,4-*syn*-diol ***dia*-92** would be favoured by DHQ ligands. The experimental results agreed with these predictions with a range of "matched" DHQD ligands enhancing the intrinsic diastereofacial selectivity (entry 2, 4, 6) while a range of "mismatched" DHQ ligands reversed the selectivity (entry 3, 5, 7).

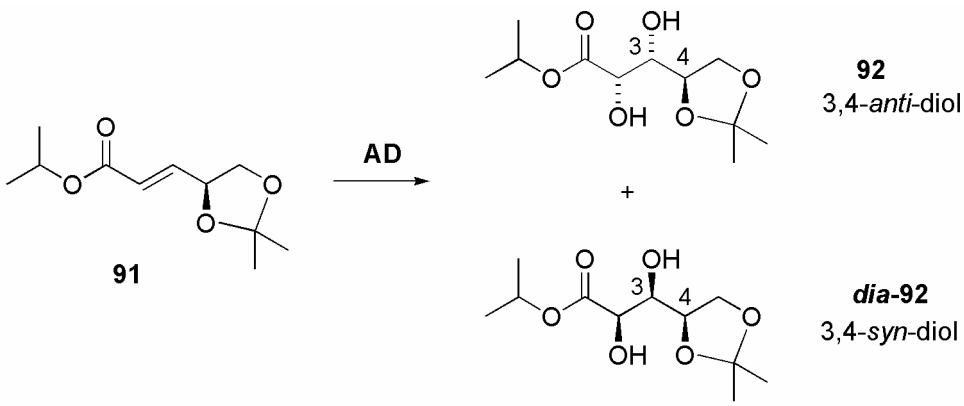

Figure 3.2 Morikawa and Sharpless's AD.

From these results it was predicted that the chiral C_3 group in alkene ***E*-23** (see Figure 3.1) would direct addition to the opposite face to favour formation of the desired 3,4-*anti*-diol **22**. The intrinsic diastereofacial selectivity of chiral alkene substrate ***E*-23** was determined to be 2 : 1 in favour of 3,4-*anti*-diol **22** by performing a reaction using catalytic osmium tetroxide with 4-methylmorpholine *N*-oxide (NMO) as the stoichiometric oxidant.

Entry	Ligand (mol%)	Ratio of **92** : ***dia*-92**	Yield (%)
1	quinuclidine (10)	2.6 : 1	85
2	DHQD-CLB (10)	10 : 1	87
3	DHQ-CLB (10)	1 : 1	85
4	$(DHQD)_2PHAL$ (1)	39 : 1.0	84
5	$(DHQ)_2PHAL$ (1)	1 : 1.3	52
6	$(DHQD)_2PYR$ (5)	6.9 : 1	90
7	$(DHQ)_2PYR$ (5)	1 : 4.1	86

Figure 3.3 Morikawa and Sharpless's results.[58]

The revised AD-mnemonic[32] (Figure 3.4) was used to predict that DHQ-derived ligands would favour addition to the desired face of alkene ***E*-23**. Positioning the alkene according to the constraints of the mnemonic, with the small hydrogen substituents of the alkene pointing towards the sterically congested southeast and northwest quadrants gives two possible substrate orientations A and B.

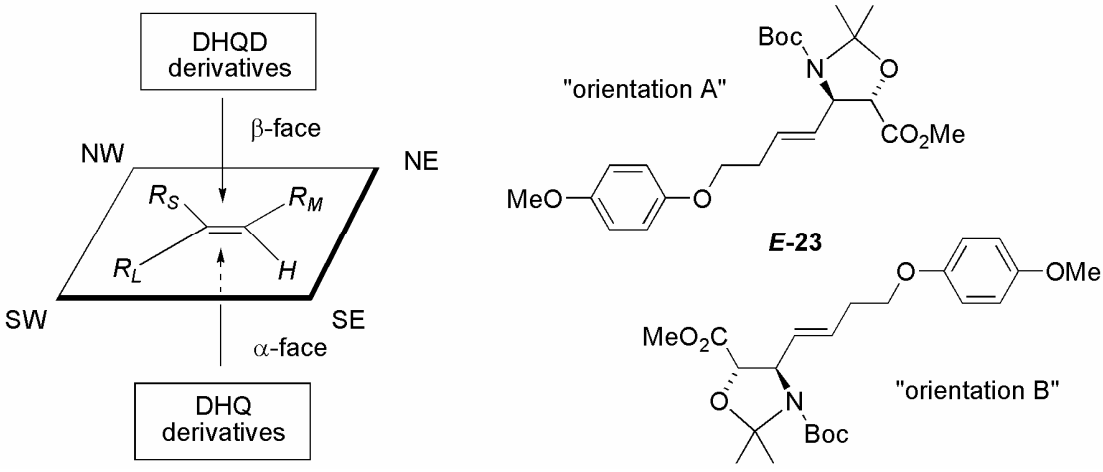

Figure 3.4 AD-mnemonic and substrate orientation.

Either orientation positions the alkene so that attack from the bottom or α-face (favoured by DHQ-derived ligands) would lead to desired 3,4-*anti*-diol **22** while

attack from the top or β-face (favoured by DHQD-derived ligands) would lead to undesired 3,4-*syn*-diol ***dia*-22**.

The phthalazine ligands have a reputation of inducing good facial selectivity in the AD of 1,2-*trans*-disubstituted alkenes and good results were obtained by Morikawa and Sharpless with these ligands (see Figure 3.3, entry 4, 5). However dihydroxylation using the recommended amounts[32] of AD-mix-α[43] containing $(DHQ)_2PHAL$ (**93** in Figure 3.5) failed to form diol products with unreacted alkene ***E*-23** recovered from the reaction after 16 h. An extended reaction time of 40 h at room temperature led to complete consumption of starting material in favour of a very polar by-product (baseline in 40% ethyl acetate : hexanes). ^1H NMR analysis identified the by-product as an alkene due to the presence of alkene-like peaks in the spectra. It was suspected that the methyl ester had been hydrolysed to the acid under the basic aqueous reaction conditions. Buffering the reaction by addition of sodium hydrogen carbonate (3.0 eq.) slowed down hydrolysis with significant alkene ***E*-23** recovered after 72 h but failed to form any diol products (Figure 3.6, entry 2). Similar results were obtained using AD-mix-β containing $(DHQD)_2PHAL$ (entry 3). It was proposed that alkene ***E*-23** was too sterically demanding to interact with the phthalazine ligands.

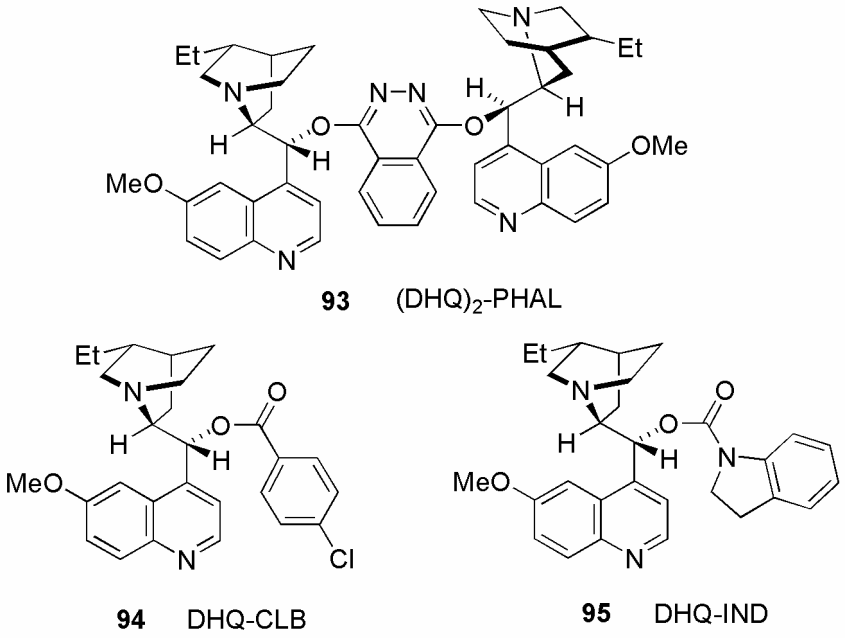

Figure 3.5 Ligands $(DHQ)_2PHAL$, DHQ-CLB and DHQ-IND.

Entry	Conditions	Temp (°C), (Time (h))	Ligand	Diol **22**	
				Yield (%)	*anti* : *syn*
1	A	RT* (2)	none	48	2.0 : 1.0
2	B	0 (5), RT* (72)	$(DHQ)_2PHAL$	0	n/a
3	B	0 (5), RT* (72)	$(DHQD)_2PHAL$	0	n/a
4	C	RT§ (17)	DHQ-CLB	11	3.3 : 1.0
5	C	RT§ (17)	DHQD-CLB	5	1.0 : 2.5
6	C	RT§ (17)	DHQ-IND	42	7.5 : 1.0
7	C	RT§ (17)	DHQD-IND	19	1.0 : 5.1
8	C#	70 (2)	DHQ-IND	70	5.1 : 1.0
9	C#	70 (2)	DHQD-IND	65	1.0 : 3.4
10	C#	RT§ (10), 27 (4)	DHQ-IND	85	7.4 : 1.0

A = OsO_4 (10 mol%) and NMO (3.3 eq.) in THF/*t*-BuOH/H_2O; **B** = AD-mix-α (entry 2) or AD-mix-β (entry 3), methanesulfonamide (1.0 eq) and $NaHCO_3$ (3.0 eq.) in *t*-BuOH/H_2O; **C** = $K_2OsO_2(OH)_4$ (1 mol%), ligand (6 mol%), $K_3Fe(CN)_6$ (3.0 eq.), K_2CO_3 (3.2 eq.), $NaHCO_3$ (3.2 eq.) and methanesulfonamide (3.2 eq.) in *t*-BuOH/H_2O at 0 °C to room temperature; ***** = performed in summer (RT ~ 28 °C); **§** = performed in winter (RT ~ 17 °C); **#** = increased reaction temperature was used

Figure 3.6 Ligand effects.

Some less sterically congested ligands were investigated employing more forcing reaction conditions recommended for sluggish substrates and tetra-substituted alkenes with increased relative amounts of reagents and increased temperatures. The reactions were buffered as previously. The monomeric ligand DHQ-CLB (**94** in Figure 3.5) gave a mixture of diol products with an enhanced *anti* : *syn* ratio (entry 4) indicating a "matched" scenario where both the ligand and the substrate are directing the addition to the same face. The pseudo-enantiomeric ligand DHQD-CLB gave a decreased ratio (entry 5) indicating a "mismatched" scenario where the ligand and the substrate are directing the addition to opposite faces. Another "matched" ligand, DHQ-IND (**95** in Figure 3.5) showed a greater enhancement of the *anti*-selectivity (entry 6) while the "mismatched" ligand, DHQD-IND showed a greater enhancement of the *syn*-

selectivity (entry 7). Typically matched scenarios give higher selectivity and sometimes higher yields than the mis-matched scenarios because the matched reaction occurs more rapidly. This was observed in the study with the matched ligands giving higher yields than the corresponding mismatched ligands under the same reaction conditions. The PHAL ligands were not used with the more forcing reaction conditions and this combination of reagents may lead to the formation of diol products.

At temperatures below 20 °C the reactions were observed to be biphasic and resulted in low yields (entry 4 – 7) with significant amounts of recovered starting alkene ***E*-23**. At temperatures above 20 °C the reaction was observed to be homogeneous. The reactions using the IND ligands were repeated at an elevated temperature of 70 °C and higher yields were obtained at the expense of selectivity (entry 8, 9). When the reaction using DHQ-IND was heated at 27 °C to imitate summer room temperature, an increased yield of 85% was obtained with only a slight decrease in selectivity (entry 10). This improved yield with good selectivity made the AD synthetically viable.

Separation of 3,4-*anti*-diol **22** from 3,4-*syn*-diol ***dia*-22** was not easily effected by flash chromatographic purification and it was hoped that minor diastereoisomer ***dia*-22** may be more conveniently removed at a later stage. No further effort was made to separate the diastereoisomers and a mixture was taken on in subsequent reactions.

3.1.2 Stereochemical Proof

The assignment of the absolute stereochemical configuration at the C_5 secondary hydroxy of 3,4-*anti*-diol **22** as (*S*) was supported by Mosher's method. It was predicted that if one equivalent of the acid was used it may be possible to selectively esterify the C_5 hydroxy which appeared to be less sterically congested than the C_4 hydroxy. Reaction using one equivalent of the acid and 1,3-dicyclohexylcarbodiimide did not afford ester products and starting diol was recovered. (*S*)-MTPA ester ***S*-96** (**Error! Reference source not found.**) was synthesised using a large excess of (*S*)-MTPA acid and unreacted diol was still recovered while formation of di-ester was not detected. An inseparable minor

isomer was detected and was assigned as the C_5-(*S*)-MTPA ester of ***dia*-22**. The (*R*)-MTPA ester ***R*-96** was synthesised by using one equivalent of (*R*)-MTPA acid chloride prepared from the acid using oxalyl chloride. Unreacted diol was recovered from the reaction and no di-ester was detected. An inseparable minor isomer was detected and was assigned as the C_5-(*R*)-MTPA ester of ***dia*-22**. The ^{1}H NMR spectra of each ester were assigned using COSY NMR and the C_5-H was found to be shifted downfield by 1.44 ppm in (*R*)-MTPA ester ***R*-96** and 1.46 ppm in (*S*)-MTPA ester ***S*-96** relative to that in diol **22**. This confirmed that esterification had occurred selectively at the C_5 hydroxy.

These esters are thought to adopt a specific conformation in solution where the carbinyl hydrogen (C_2-H), trifluoromethyl group and ester carbonyl of the MTPA moiety line up in the same plane (the plane of the page in **Error! Reference source not found.**). The phenyl of the MTPA ester shields protons that are on the same side of the plane as it. If C_5 had the predicted (*S*)-configuration the signals due to the protons of the C_1 to C_4 region of the molecule would be shielded in (*R*)-Mosher ester ***R*-96** relative to that in (*S*)-Mosher ester ***S*-96** giving a negative chemical shift difference ($\Delta\delta$ where $\Delta\delta = \delta_R - \delta_S$ in ppm). The protons of the C_6 to C_7 would be shielded in ester ***S*-96** relative to that in ester ***R*-96** giving a positive $\Delta\delta$. If C_5 had an (*R*)-configuration the opposite shielding would be observed.

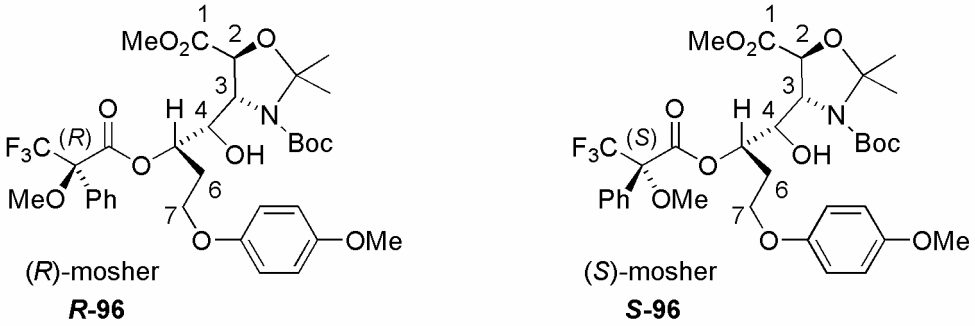

Figure 3.7 Mosher's esters of AD product.

The ^{1}H NMR spectra of the esters were assigned using COSY correlations and the chemical shift differences were calculated (**Error! Reference source not found.**). The arrangement of positive and negative $\Delta\delta$'s supports the assignment of C_5 as the (*S*)-configuration. The configuration at C_4 was assigned as (*S*)-

because the AD is known to install an aminoalcohol *via* a concerted *syn* addition with complete stereo-specificity.

Proton	δ_R (*R*)-MTPA ester ***R*-96**	δ_S (*S*)-MTPA ester ***S*-96**	$\Delta\delta$ (δ_R-δ_S)
CO_2CH_3	3.77	3.77	0.00
C_2-H	4.85	4.84	+0.01
C_3-H	4.46	4.50	-0.04
BOC $C(CH_3)_3$	1.48	1.49	-0.01
C_4-H	4.20 – 4.12	4.17	-0.01*
C_6-H_A	2.42 – 2.29	2.36 – 2.22	+0.07*
C_6-H_B	2.21 – 2.11	2.15 – 1.98	+0.10*
C_7-H_2	4.09 – 3.97	3.95 – 3.81	+0.15*
Ar-H	6.81	6.85 – 6.76	+0.01
Ar-OCH_3	3.77	3.77	0.00

* = $\Delta\delta$ was calculated from the midpoints of the multiplets

Figure 3.8 Relative shifts in the 200 MHz ^{1}H NMR spectra of Mosher's esters **96**.

In summary, the desired 3,4-*anti*-diol **22** was formed using DHQD-IND in good yield with good diastereoselectivity.

3.2 Elaboration to Aldehyde 19

Protection of diol **22** as acetal **97** proceeded smoothly in excellent yield (Figure 3.9). Subsequent de-protection of the aromatic ether using cerium ammonium nitrate (CAN) with an optimised reaction time of 18 min, afforded alcohol **98**. Shorter reaction times resulted in recovery of significant starting material while extended reaction times led to decomposition products. Oxidation of purified alcohol **98** with freshly prepared Dess-Martin periodinane afforded aldehyde **19** in quantitative crude yield.

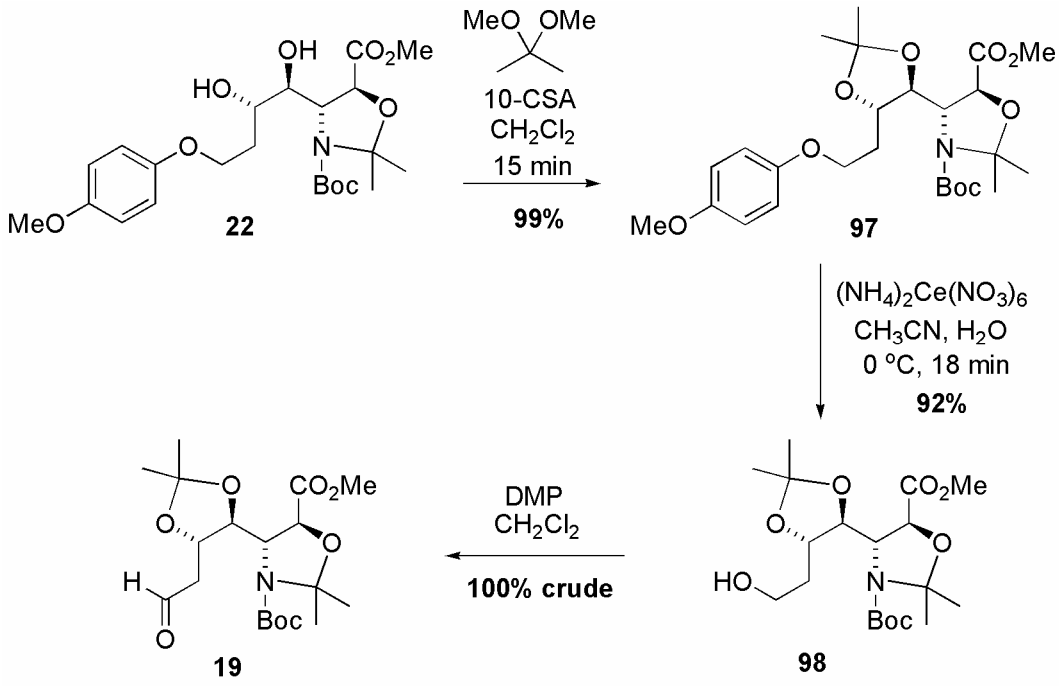

Figure 3.9 Elaboration to aldehyde **19**.

3.3 The Final Step

3.3.1 Julia Olefination

An introduction to the modified Julia olefination was given in Chapter 2 (page **Error! Bookmark not defined.**). The proposed reaction (Figure 3.10) involves reaction of sulfone **21** with a base and aldehyde **19** to form alkene **18**. According to Blakemore's summary of selectivity (see Chapter 2, page **Error! Bookmark not defined.**) β,γ-unsaturated sulfone **21** would be expected to react with aliphatic aldehyde **19** via path **B** to form alkene **18** with low to moderate (*Z*)-selectivity.

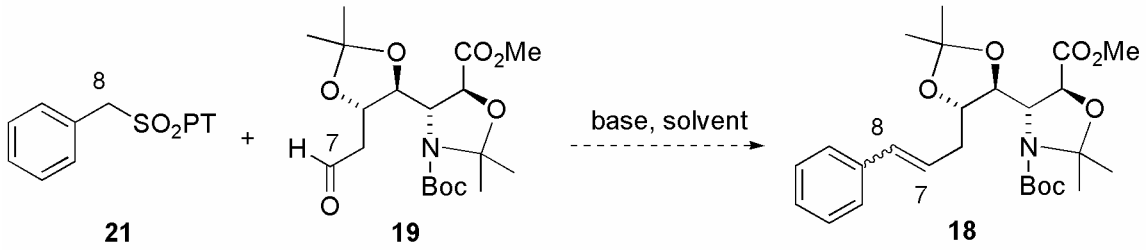

Figure 3.10 Proposed Wittig olefination.

The required PT-hetero-aromatic sulfone **21**[75] was prepared from benzyl alcohol **99** in 2 steps (Figure 3.11). Mitsunobu reaction between benzyl alcohol **99** and 1-phenyl-1*H*-tetrazole-5-thiol (PT-SH) gave thio-ether **100**[74] and subsequent oxidation gave sulfone **21**. The oxidation reaction was monitored by TLC and the formation and subsequent disappearance of a more polar compound was observed. When the reaction was stopped prematurely intermediate sulfoxide **101** was isolated.

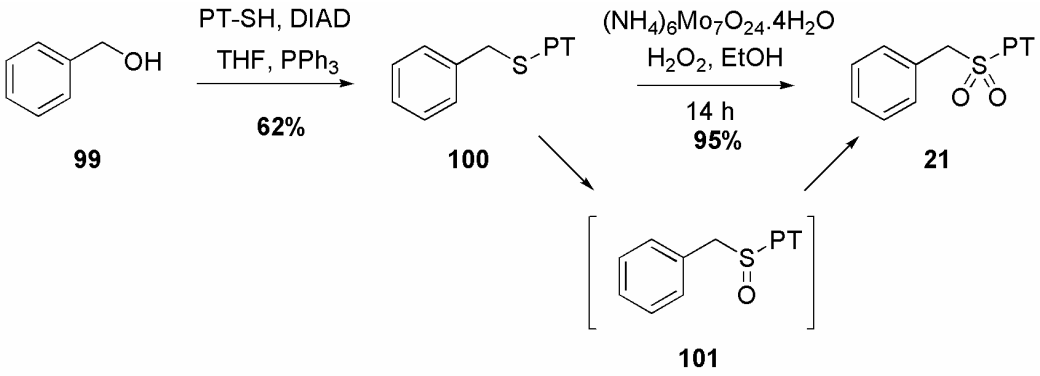

Figure 3.11 Preparation of sulfone **21**.

Model reaction of PT-sulfone **21** with isobutyraldehyde **88** and different bases under premetallation conditions were carried out to form alkene **102**[78,79] (Figure 3.12). The reaction yield was not determined because alkene **102** was volatile and the selectivity was determined by ^{1}H NMR analysis of the crude product. The reaction favoured formation of (*Z*)-alkene ***Z*-102** (Figure 3.13, entries 1, 2). The model studies were repeated with heptaldehyde **103** to form alkene **104**[80] and similar (*Z*)-selectivity was observed (entries 3, 4). It was interesting to note that with isobutyraldehyde **88**, KHMDS gave a decreased (*Z*)-selectivity while with heptaldehyde **103**, *n*-BuLi gave a decreased (*Z*)-selectivity. The low (*Z*)-selectivity in these reactions is in agreement with Blakemore's summary of selectivity.

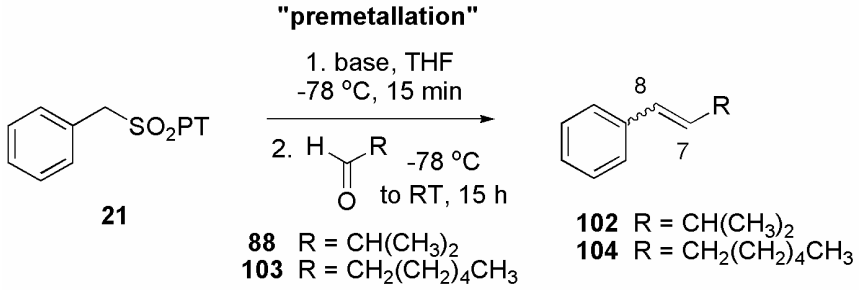

Figure 3.12 Models of final Julia olefination.

Entry	Base	Aldehyde	Alkene	*E* : *Z**
1	*n*-BuLi	**88**	**102**	1.0 : 4.0
2	KHMDS	**88**	**102**	1.0 : 2.0
3	*n*-BuLi	**103**	**104**	1.0 : 1.6
4	KHMDS	**103**	**104**	1.0 : 2.1

* = determined by integration of the C_7-H and C_8-H peaks in the 200 MHz ^{1}H NMR spectra of the crude product

Figure 3.13 Results of model studies.

In both model studies no unreacted sulfone **21** was recovered and unidentified by-products, presumed to be self-condensation products, were observed. In reactions using the nucleophilic base *n*-BuLi, analysis of the crude product by ^{1}H NMR suggested the formation of by-product **105**, presumed to be due to butyl addition at the *ipso*-position of the sulfone.

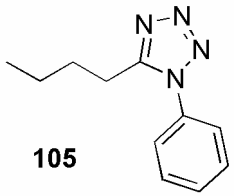

105

Figure 3.14 By-product **105**.

It was predicted from the model studies that the best results would be obtained using the non-nucleophilic base KHMDS with Barbier conditions however low (*Z*)-selectivity was expected. A small scale Julia olefination was performed using aldehyde **19**. The conditions used were influenced by the results of both the model study and the Julia olefination to form alkene **23** (see Chapter 2). Barbier addition using KHMDS as the base and 1,2-dimethoxyethane as the solvent failed to form alkene products. Some unreacted sulfone was recovered while no residual aldehyde was recovered.

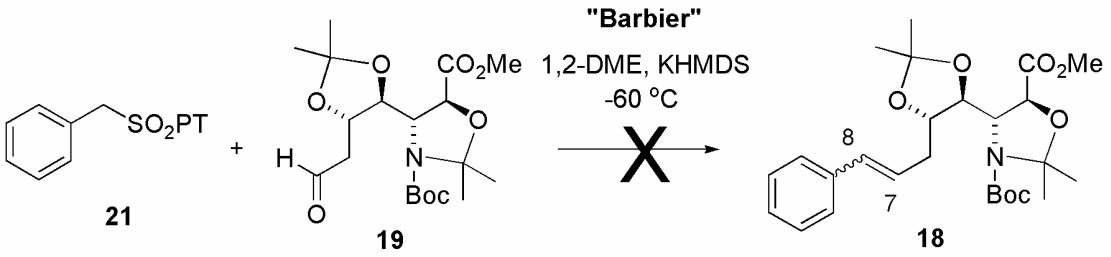

Figure 3.15 Final Julia olefination.

It was decided to abandon this reaction as a means of installing the aromatic tail due to poor reactivity and poor (*E*)-selectivity displayed in the model study. Alternative methods using HWE olefination and Wittig olefination were pursued.

3.3.2 Horner-Wadsworth-Emmons Olefination

An introduction to the HWE olefination was given in Chapter 2 (page **Error! Bookmark not defined.**). The HWE olefination is generally very (*E*)-selective and it was hoped that better (*E*)-selectivity could be seen using this method. The proposed reaction (Figure 3.16) involves formation of the anion of phosphonate **106** by reaction with base and subsequent addition to aldehyde **19** to form alkene **18**.

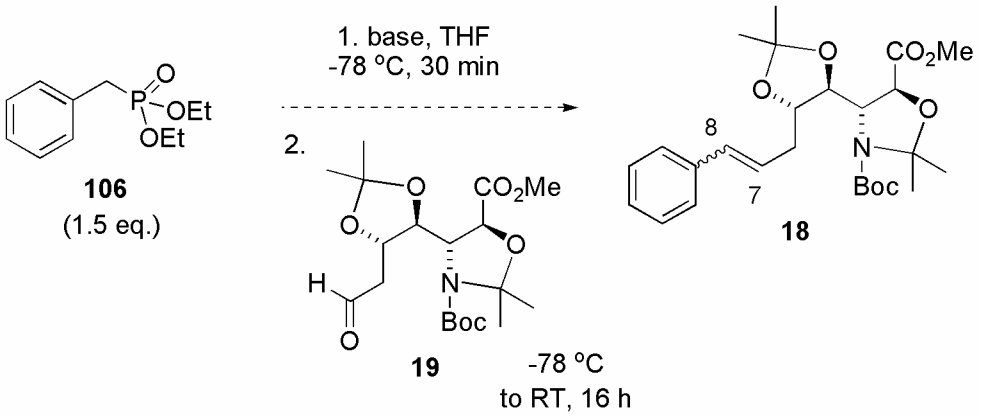

Figure 3.16 Proposed HWE reaction.

Phosphonate **106**[76] was prepared by reacting benzyl bromide **107** with triethyl phosphite (Figure 3.17) and the product was purified by fractional distillation.

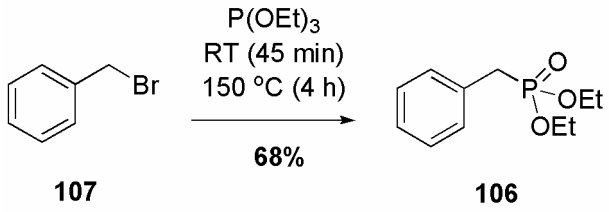

Figure 3.17 Preparation of phosphonate **106**.

Model reactions of phosphonate **106** with different bases and isobutyraldehyde **88** were performed (Figure 3.18). The reaction using *n*-BuLi formed (*E*)-alkene ***E*-102** exclusively (Figure 3.19, entry 1) while KHMDS favoured the formation of (*E*)-alkene to a lesser extent (entry 2). The model study was repeated using heptaldehyde **103** with KHMDS to form alkene **104** and a similar (*E*)-selectivity was observed (entry 3). Significant amounts of unreacted phosphonate **106** were seen in the crude ^{1}H NMR of these reactions but no unreacted aldehyde was observed. Warming the reaction to room temperature after the addition of base and before addition of the aldehyde failed to improve conversion.

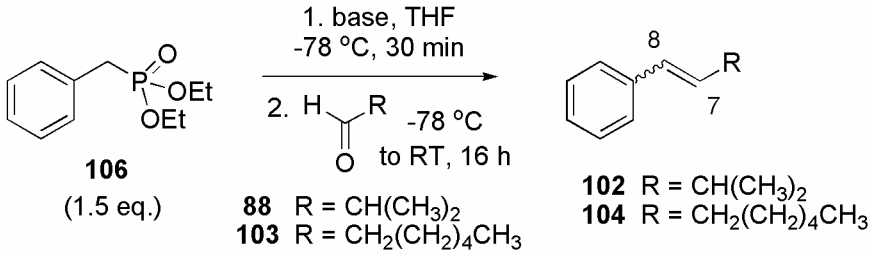

Figure 3.18 Model HWE olefination.

Entry	Base	Aldehyde	Alkene	*E* : *Z* : **106***
1	*n*-BuLi	**88**	**102**	1.0 : 0 : 3.3
2	KHMDS	**88**	**102**	4.4 : 1 : 3.1
3	KHMDS	**103**	**104**	3.2 : 1 : 32

* = determined by integration of the C_7-H and C_8-H peaks in the 200 MHz ^{1}H NMR spectra of the crude product

Figure 3.19 Results of model HWE olefination.

From the model study the HWE olefination was predicted to give good (*E*)-selectivity in the actual reaction. HWE olefination between the ylide formed by

reaction of phosphonate **106** with KHMDS and aldehyde **19** gave only unidentified decomposition products and recovered phosphonate **106**. It was suspected that the metallate of the phosphonate was too basic for reaction with functionalised aldehyde **19** and this approach was abandoned. Focus was turned to the Wittig olefination.

3.3.3 Wittig Olefination

An introduction to the Wittig olefination was given in Chapter 2 (page **Error! Bookmark not defined.**). The proposed reaction (Figure 3.20) involves formation of the ylide of phosphonium salt **20** by reaction with base and subsequent addition of aldehyde **19** to form alkene **18**. The phosphorus ylide of phosphonium salt **20** is partially stabilised but still needs to be formed *in situ* by treatment of the phosphonium salt with a base.

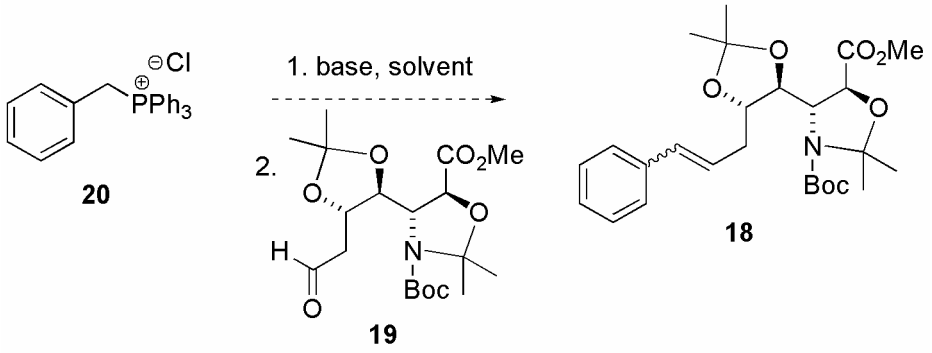

Figure 3.20 Proposed Wittig olefination.

Phosphonium salt **20**[77] was prepared by reaction of triphenylphosphine with benzyl chloride **108** (Figure 3.21). The salt was a white powder which was not especially hygroscopic but was stored under vacuum over potassium hydroxide before use.

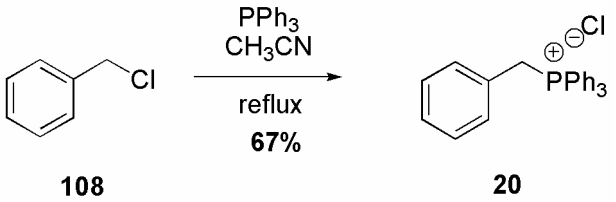

Figure 3.21 Preparation of phosphonium salt **20**.

At this stage the isobutyraldehyde model had been abandoned due to product volatility however for comparison with the previous models a Wittig olefination between phosphonium salt **20** and isobutyraldehyde **88** was conducted (Figure 3.22). Reaction of phosphonium salt **20** with *n*-butyl lithium to form ylide **109** *in situ* followed by addition of isobutyraldehyde **88** formed alkene **102**. The product was isolated with minimal evacuation under reduced pressure and the selectivity was determined by ^{1}H NMR analysis. The product was formed with an *E* : *Z* ratio of 4 : 1 however significant unreacted phosphonium salt **20** was detected in the crude product mixture. (Figure 3.23, entry 1). A solubility study of phosphonium salt **20** was conducted and it was found to be not very soluble in tetrahydrofuran, partially soluble in toluene and completely soluble in benzene. It was decided that benzene would be a better solvent for subsequent reactions.

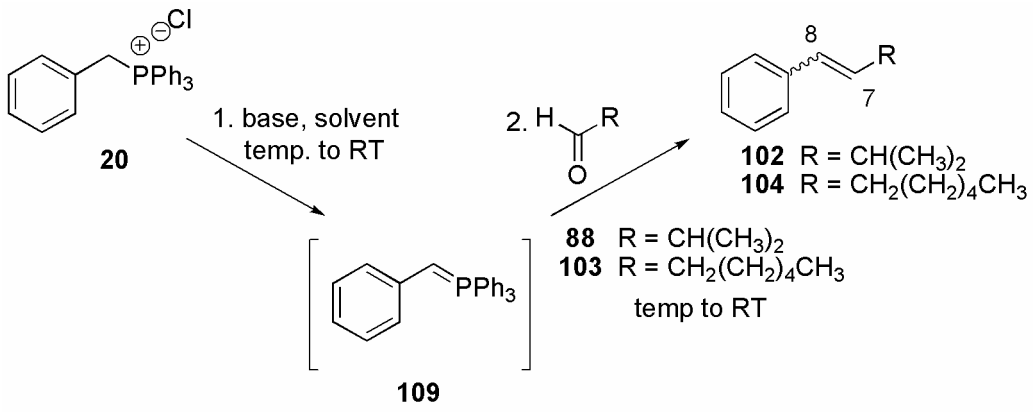

Figure 3.22 Model Wittig reaction.

Entry	Equiv. of **20**	Base (equiv.)	Solvent	Temp (℃)	Aldehyde, Alkene	Yield (%)	*E* : *Z* : **20***
1	1.5	*n*-BuLi (1.2)	THF	-78	**88**, **102**	§	4.0 : 1 : 4.0
2	1.0	*n*-BuLi (1.0)	benzene	0	**103**, **104**	58	3.0 : 1 : 1.3
3	1.0	KHMDS (1.0)	benzene	0	**103**, **104**	75	3.0 : 1 : 0.5

* = determined by integration of the C_7-H and C_8-H peaks in the 200 MHz ^{1}H NMR spectra of the crude product; **§** = not determined

Figure 3.23 Results of model Wittig olefinations.

Model reactions between phosphonium salt **20** and heptaldehyde **103** using *n*-BuLi (entry 2) and KHMDS (entry 3) were performed. Both bases showed the same (*E*)-selectivity however better yield and conversion were obtained using KHMDS. From the model studies the Wittig olefination between phosphonium salt **20** and aldehyde **19** was expected to give much better (*E*)-selectivity that the modified Julia olefination and better conversion than the HWE olefination.

Wittig olefination between phosphonium salt **20** and aldehyde **19** worked well to form a mixture of (*E*)-alkene ***E*-18** and (*Z*)-alkene ***Z*-18** in a 3.5 : 1 ratio and 77% isolated yield (Figure 3.24). The isomers were not easily separated by flash chromatography. Preparative HPLC was used to separate the isomers and to remove trace impurities that were assumed to be alkene products with opposite diol stereochemistry.

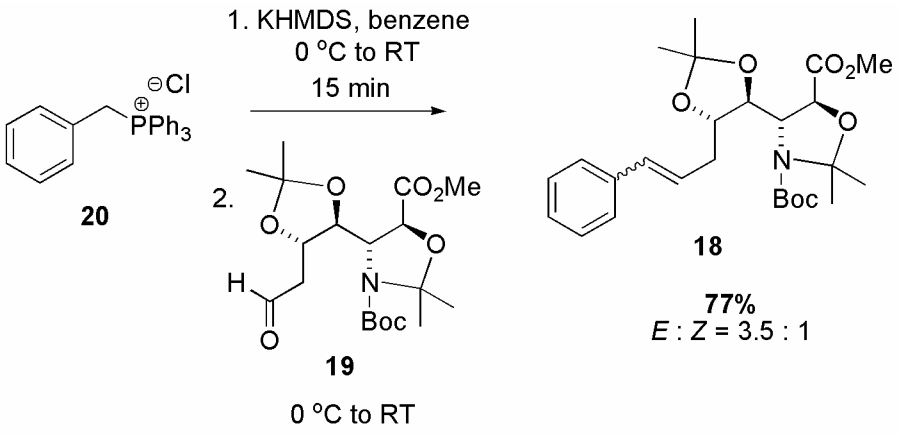

Figure 3.24 Wittig olefination to alkene **18**.

Protected APTO ***E*-18** was synthesised in fourteen linear steps and an overall yield of 11%. This is the first synthesis to date of a protected form of APTO precursor. The synthesis is short with a unique combination of AA and AD reactions that could be used to target the various poly-hydroxylated amino acid derivatives present in the other members of the microsclerodermin family. The project now turned to address the synthesis of AETD, the closest analogue of APTO.

3.4 Application of the strategy to AETD

It was envisaged that the same synthetic strategy could be applied to the synthesis of AETD by coupling late-stage common precursor aldehyde **19** with the ylide of phosphonium salt **29** to form alkene **30** (Figure 3.25). The phosphorus ylide of phosphonium salt **29** is partially stabilised but needs to be formed *in situ* by treatment of the salt with a base.

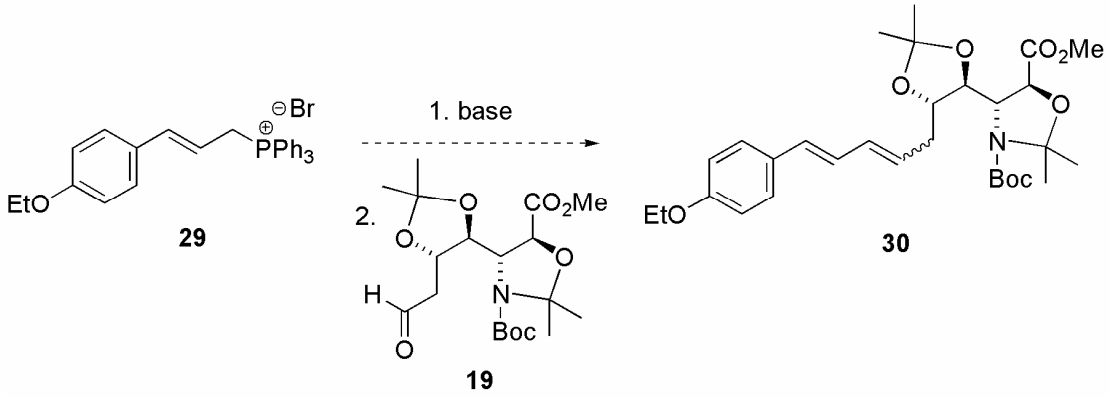

Figure 3.25 Proposed Wittig olefination to form alkene **30**.

Phosphonium salt **29** was prepared in three steps from commercially available ethyl *trans*-4-ethoxycinnamate **110** (Figure 3.26). Reduction of ethyl *trans*-4-ethoxycinnamate **110** with diisobutylaluminium hydride (DIBAL-H) proceeded smoothly to afford alcohol **111**[81]. Bromine substitution was attempted using triphenylphosphine dibromide via the methods of White et al.[59] which formed bromide **112** contaminated with unknown impurities. Attempts to purify the bromide by flash chromatography led to extensive decomposition and the reaction could not be monitored by TLC due to extensive streaking. Effective bromine substitution was achieved using phosphorus tribromide to afford pure bromide **112** and further purification was not necessary. Bromide **112** was combined with triphenylphosphine to form phosphonium salt **29** in excellent overall yield. The salt was stored under reduced pressure over potassium hydroxide before use in subsequent Wittig olefinations.

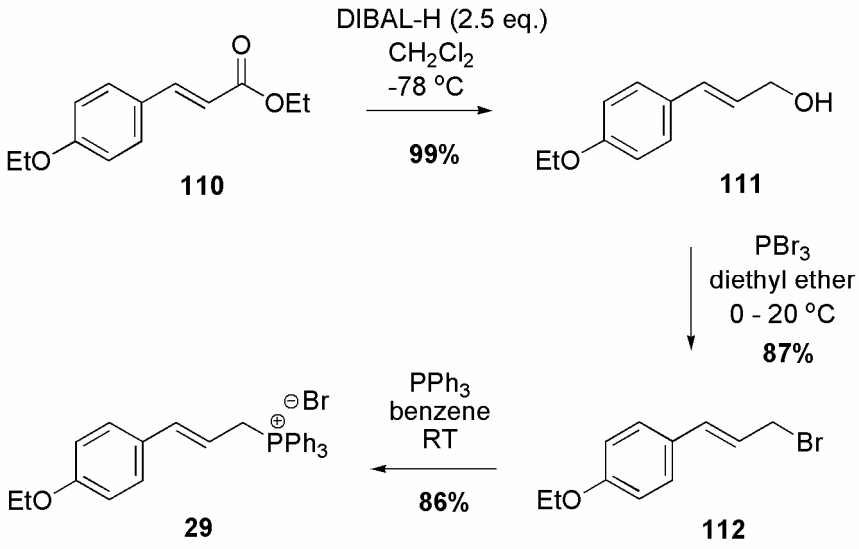

Figure 3.26 Formation of phosphonium salt **29**.

A model Wittig olefination (Figure 3.27) was conducted by reaction of phosphonium salt **29** with base to form ylide **113** *in situ* followed by addition of isobutyraldehyde **88** to form a mixture of (*E*,*E*)-diene ***E*-114** and (*E*,*Z*)-diene ***Z*-114**. The model reaction worked well using either *n*-BuLi (Figure 3.28, entry 1) or KHMDS (entry 2) as the base. KHMDS gave a slightly lower yield but gave better (*E*)-selectivity making it the base of choice.

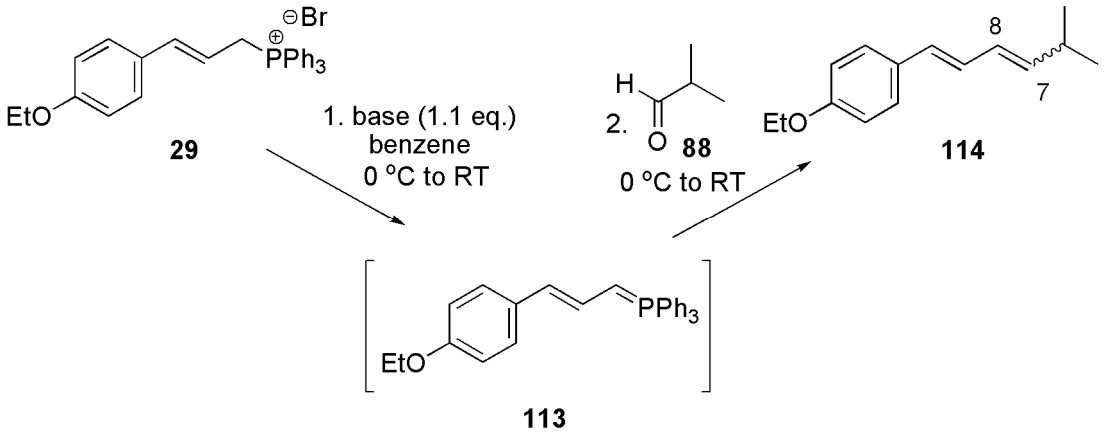

Figure 3.27 Model Wittig olefination.

Diene **114** was found to be quite unstable decomposing on the bench overnight or after four days in a freezer. LRMS analysis at the usual energy of 70 eV did not give any peaks and using a lower energy (40 eV) gave a broad evaporation chromatogram indicating possible decomposition. The resulting spectra contained peaks corresponding to M^+, $2M^+$, $3M^+$ and other peaks of equal distance apart

(56 amu) which may indicate polymerisation. Full characterisation data were not obtained due to decomposition however all spectral data obtained were consistent with the proposed structure.

Entry	Base	Diene **114**	
		Yield (%)	*E* : *Z**
1	*n*-BuLi	80	1.7 : 1.0
2	KHMDS	75	2.5 : 1.0

* = determined by integration of the C_7-H and C_8-H peaks in the 200 MHz ^{1}H NMR spectra of the crude product

Figure 3.28 Results of model Wittig olefinations.

Wittig olefination between phosphonium salt **29** and aldehyde **19** worked well forming a mixture of (*E*,*E*)-diene ***E*-30** and (*E*,*Z*)-diene ***Z*-30** in a 3.2 : 1 ratio and with an isolated yield of 63% (Figure 3.29). The isomers were not easily separated by flash chromatography. Preparative HPLC was used to separate the isomers and to remove trace impurities that were assumed to be alkene products with opposite diol stereochemistry. Both dienes were heated overnight at 340 K to acquire good characterisation NMR data. During this time significant decomposition occurred to (*E*,*Z*)-diene ***Z*-30** and to a lesser extent with (*E*,*E*)-diene ***E*-30**.

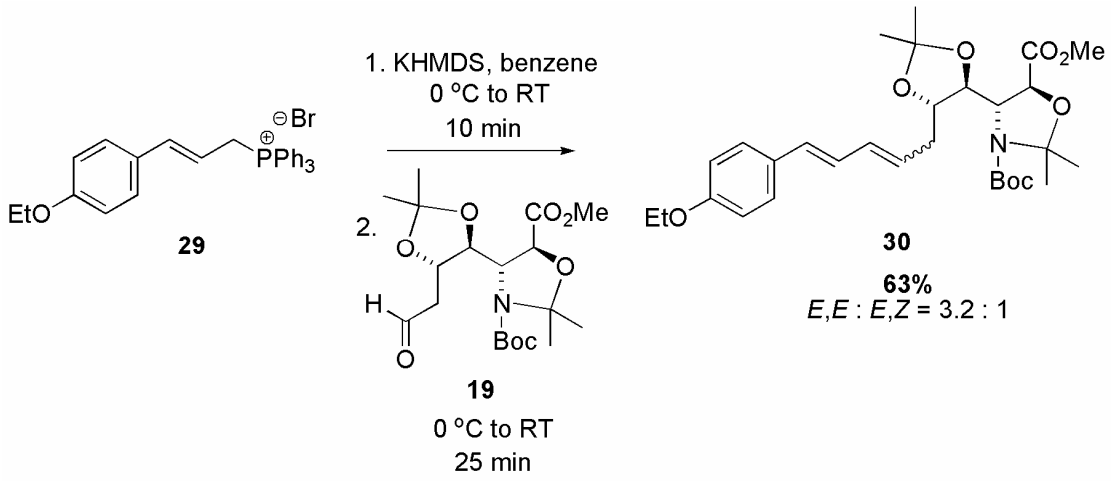

Figure 3.29 Wittig olefination to AETD.

Protected AETD ***E*-30** was synthesised in fourteen linear steps and an overall yield of 8%. This is the second synthesis to date of a protected AETD precursor and is effected in fewer steps and greater overall yield compared to the first, published by Jidong Zhu and Dawei Ma (for a summary of Zhu and Ma's synthesis, see Chapter 1, page **Error! Bookmark not defined.**).[24]

During the course of these syntheses some alternative protecting group strategies and procedure modifications were addressed. An account of these is given in the next chapter.